

Ivanova *et al.* SUPPORTING INFORMATION FILE

Stabilization of lead-free bulk CsSnI₃ perovskite thermoelectrics via incorporating TiS₃ nanoribbon clusters

Alexandra Ivanova,^{1,*} Lev Luchnikov,¹ Dmitry S. Muratov,² Margarita Golikova,¹ Danila Saranin,¹ Aleksandra Khanina,¹ Pavel Gostishchev¹ and Vladimir Khovaylo¹

¹ National University of Science and Technology MISIS (NUST MISIS), Leninsky av. 4, Moscow, 119049, Russia

² Chemistry Department, University of Turin, 10125, Turin, Italy

* Corresponding author. E-mail address: aivanova@misis.ru (A. Ivanova).

XRD data

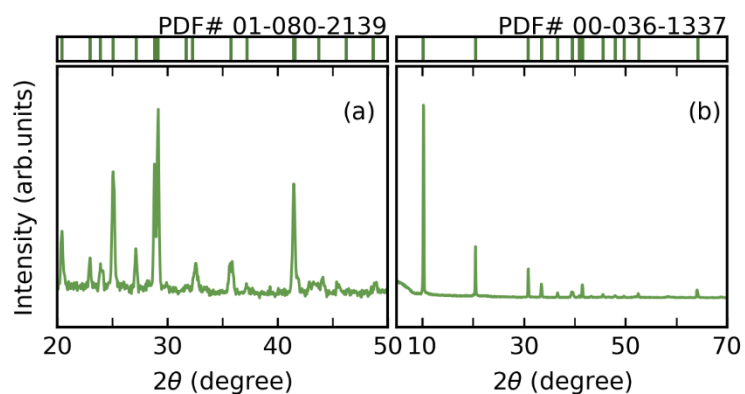


Fig.S1. PXRD patterns for (a) CsSnI_3 and (b) TiS_3 after synthesis.

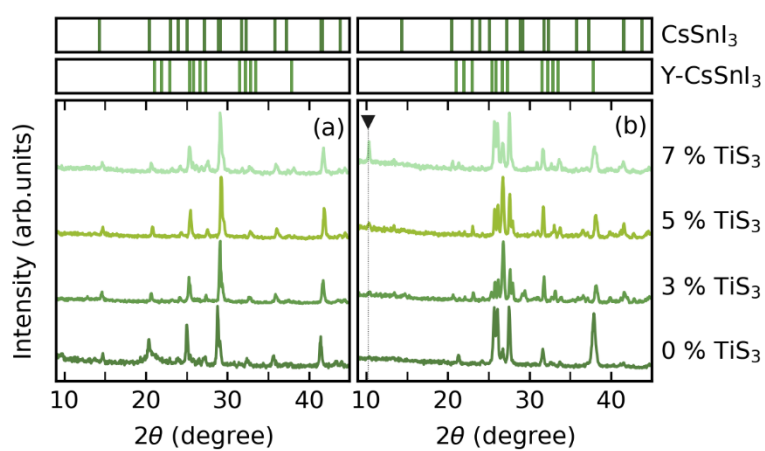


Fig.S2. XRD patterns (a) of the surfaces of bulk samples and (b) of the milled samples after pressure-less sinter.

Raman data

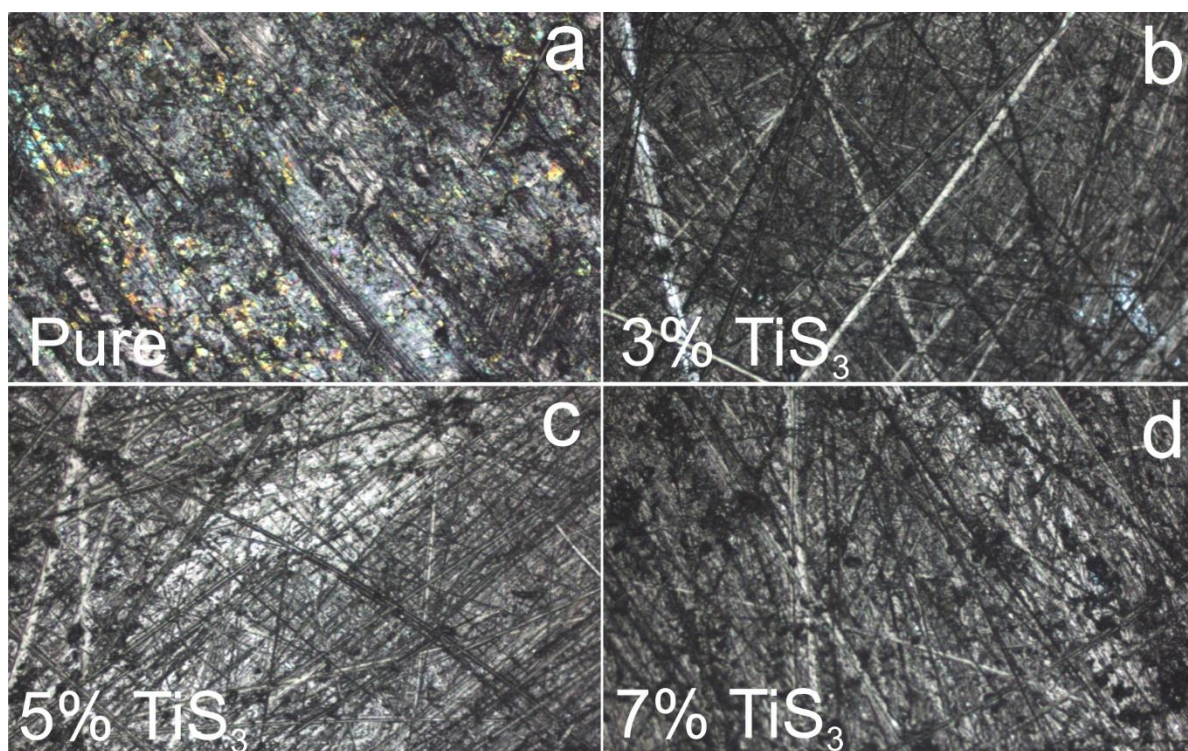


Fig.S3. Microphotography with magnification x20 of CsSnI₃ tablets surfaces after 24h air exposure.

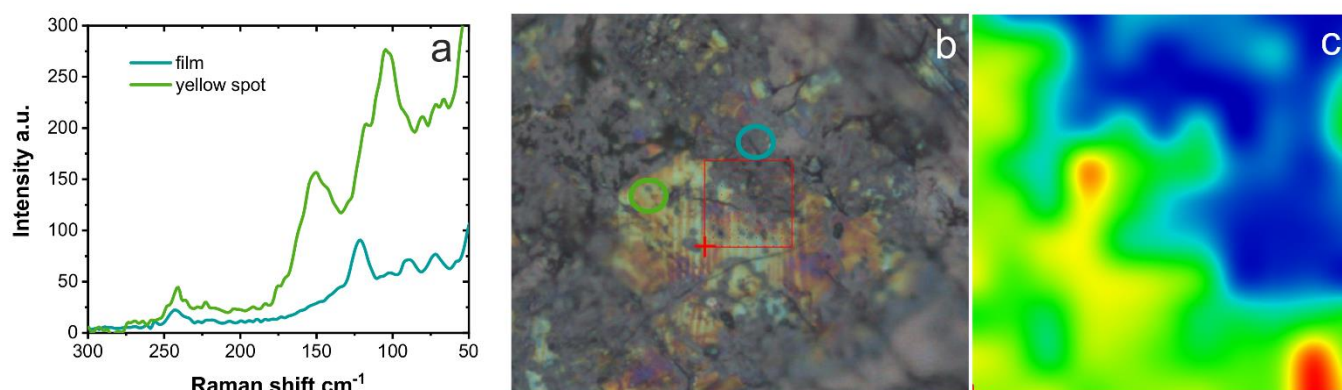


Fig.S4. Raman spectra (a) and raman map (b,c) of yellow-black region on surface of pure CsSnI₃ tablet after 24 air exposure.

SEM images and EDX mapping

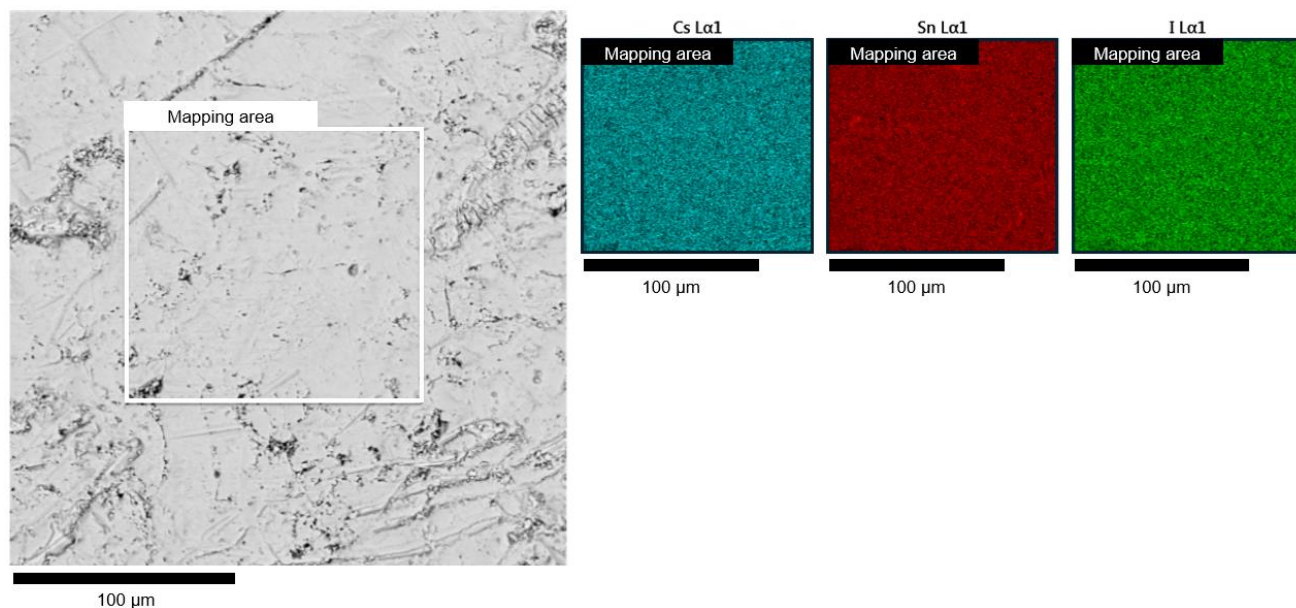


Fig. S5. SEM image of the polished surface of the CsSnI_3 without air exposure specimen and corresponding EDX maps.

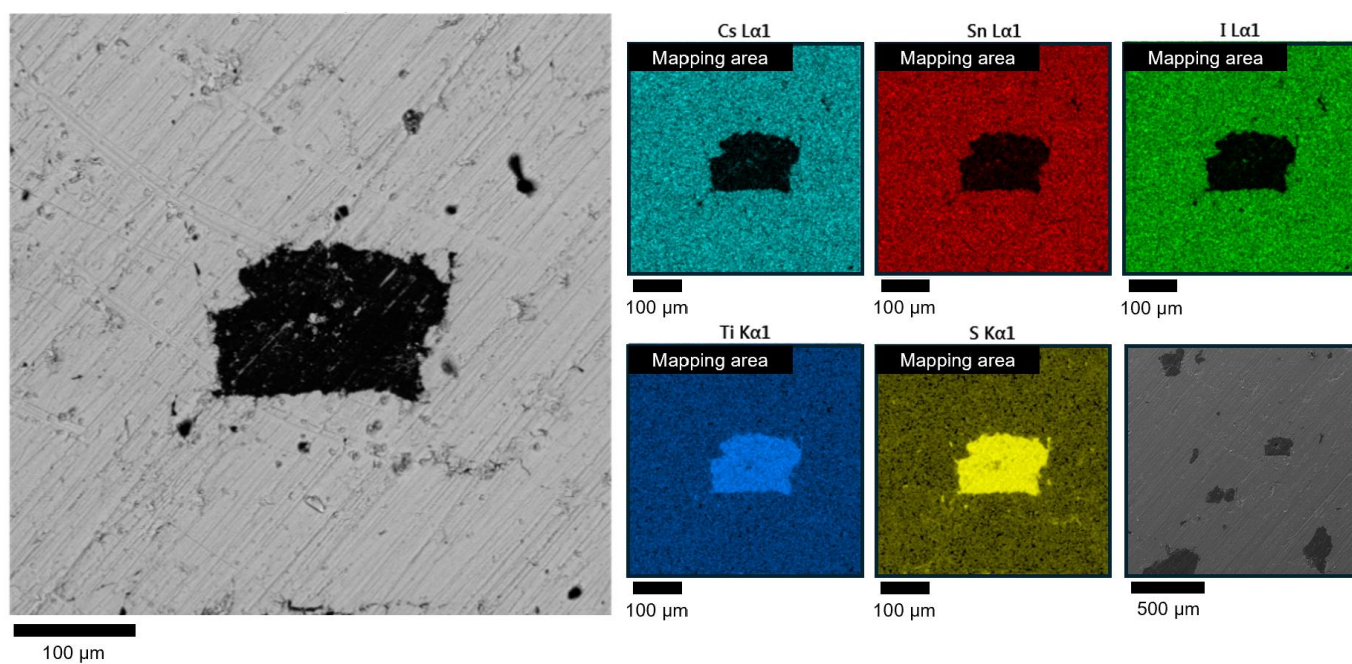


Fig. S6. SEM image of the polished surface of the CsSnI_3 + 3 wt. % TiS_3 without air exposure specimen and corresponding EDX maps.

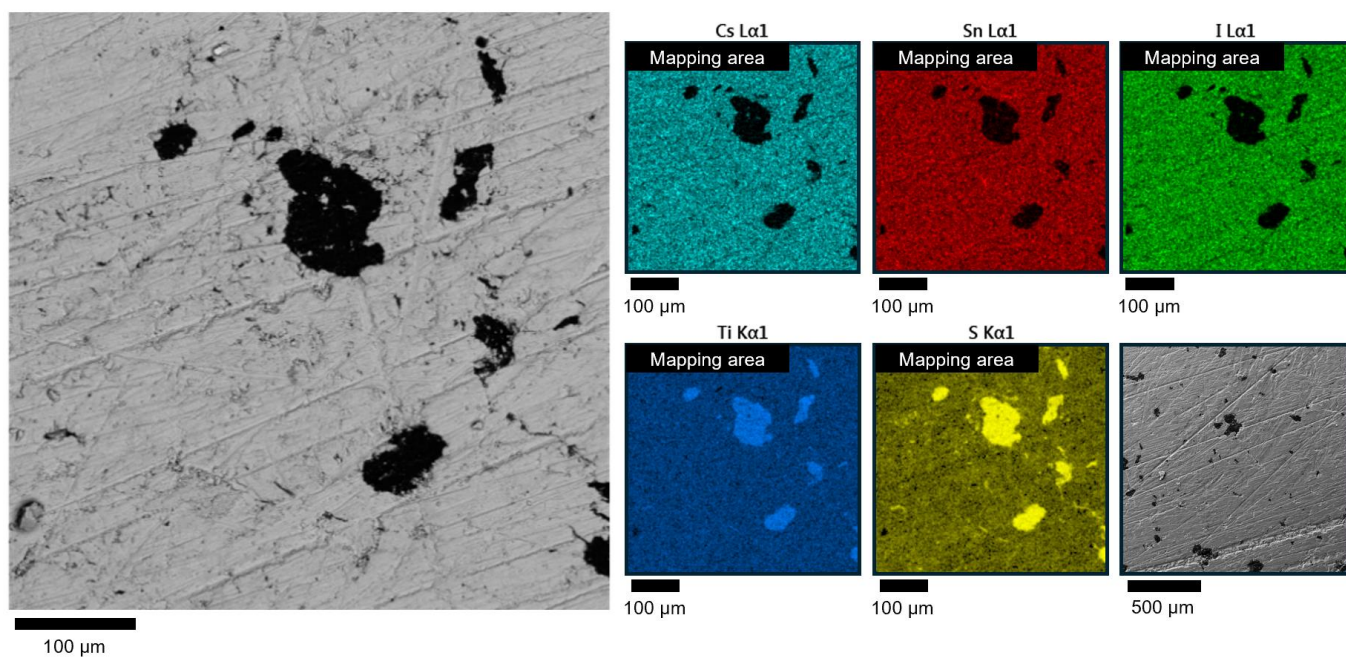


Fig. S7. SEM image of the polished surface of the $\text{CsSnI}_3 + 5 \text{ wt. \% TiS}_3$ without air exposure specimen and corresponding EDX maps.

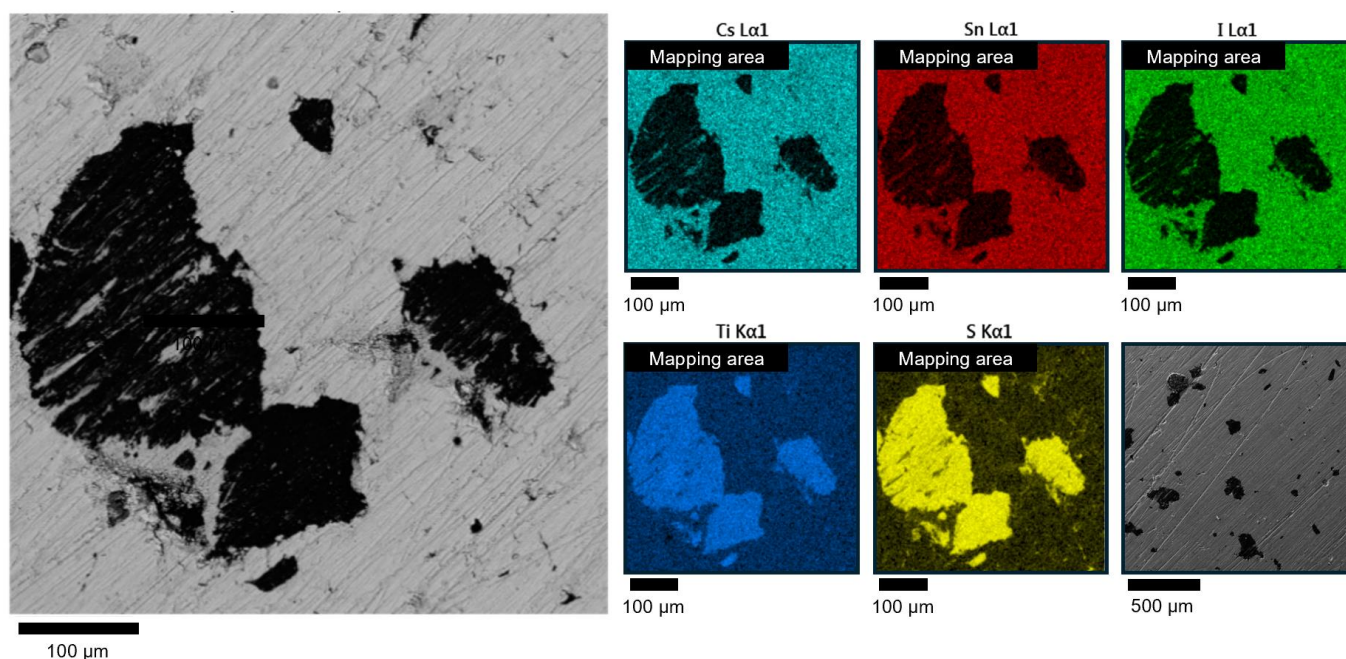


Fig. S8. SEM image of the polished surface of the $\text{CsSnI}_3 + 7 \text{ wt. \% TiS}_3$ without air exposure specimen and corresponding EDX maps.

XRD data and EDX data

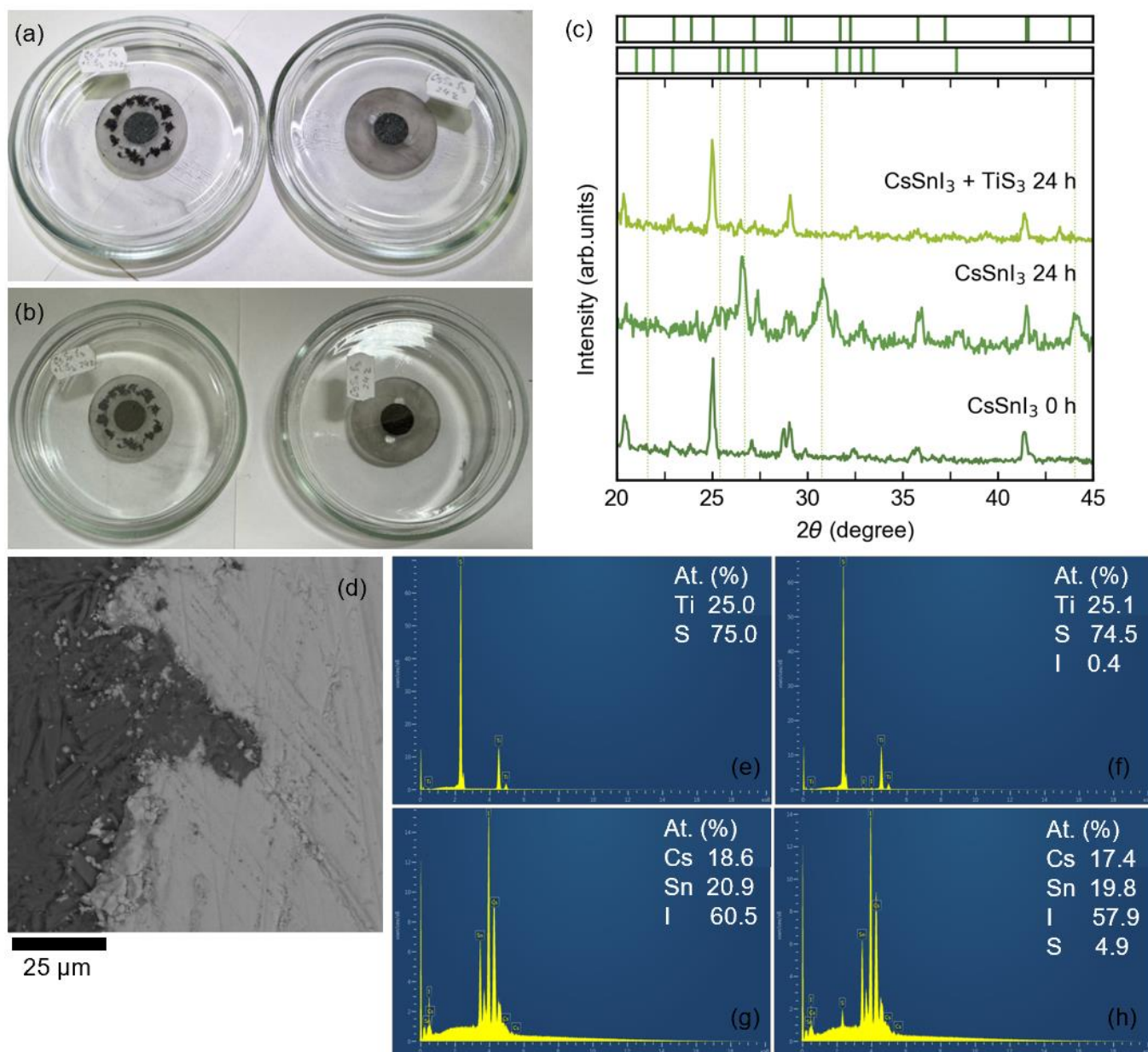


Fig. S9. Photos of prepared powders (a) after 5 hours in the box and (b) 24 hours in the air, (c) XRD of these powders, (d) SEM image of the sample $\text{CsSnI}_3 + 15 \text{ wt.}\% \text{ TiS}_3$, EDX spectrum analysis (e) of pure TiS_3 , (f) near the grain boundaries on TiS_3 side, (g) of pure CsSnI_3 , (h) near the grain boundaries on CsSnI_3 side (atomic %).

Electrical transport properties

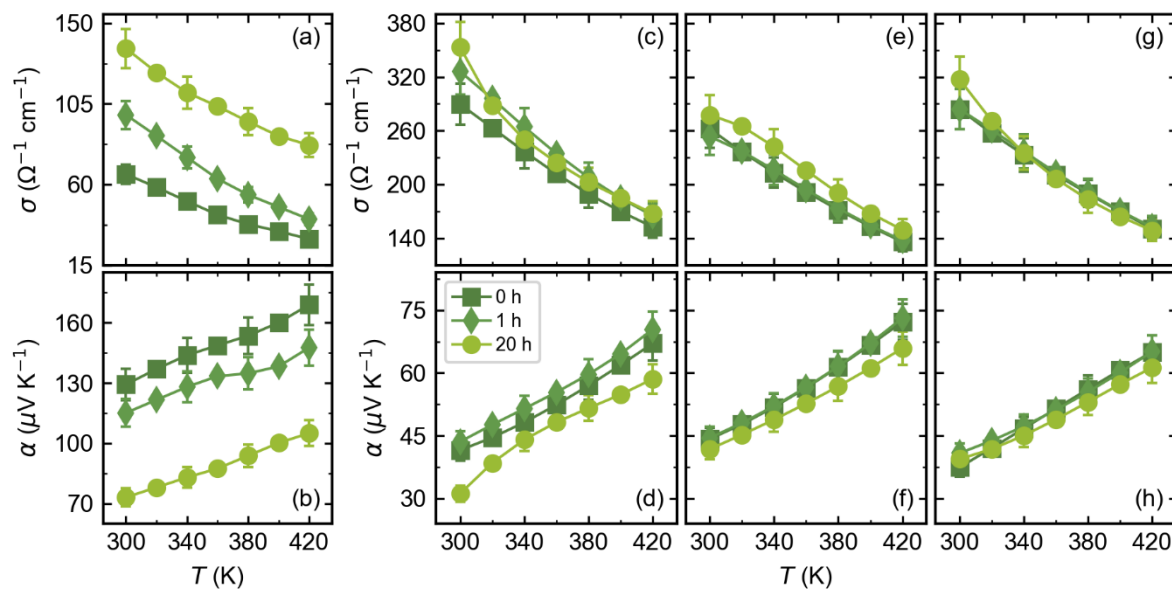


Fig. S10. Temperature dependence of electrical conductivity σ and Seebeck coefficient α of (a, b) CsSnI_3 , (c, d) $\text{CsSnI}_3 + 3$ wt.% TiS_3 , (e, f) $\text{CsSnI}_3 + 5$ wt.% TiS_3 , (g, h) $\text{CsSnI}_3 + 7$ wt.% TiS_3 .

Thermal transport properties

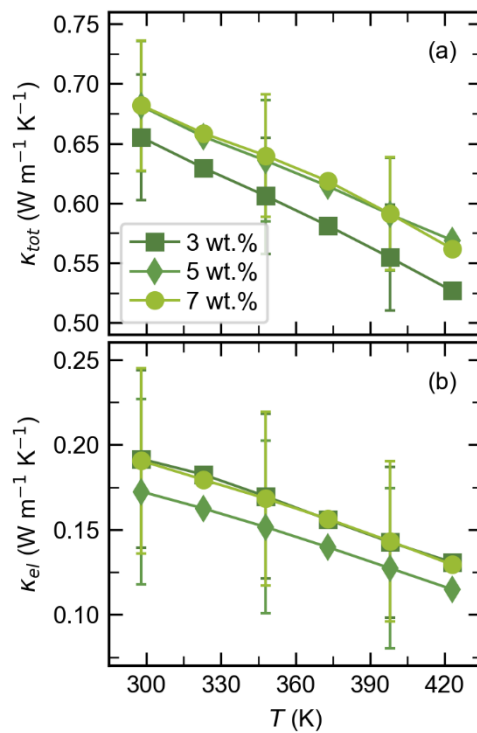


Fig. S11. Temperature dependence of (a) the total thermal conductivity and (b) the electrical thermal conductivity of the $\text{CsSnI}_3 + x \text{ wt.\% TiS}_3$ ($x = 3, 5$ and 7 wt.\%)